Review Article

Nano Research
2023, 16(11): 12572–12578

ISSN 1998-0124 CN 11-5974/O4
https://doi.org/10.1007/s12274-023-6256-z

Carbon nanotubes as outstanding targets for laser-driven particle acceleration

Wenjun Ma[1,2,3] (✉)

[1] *State Key Laboratory of Nuclear Physics and Technology, and Key Laboratory of HEDP of the Ministry of Education, CAPT, Peking University, Beijing 100871, China*
[2] *Beijing Laser Acceleration Innovation Center, Beijing 101400, China*
[3] *Institute of Guangdong Laser Plasma Technology, Guangzhou 510540, China*

Received: 3 September 2023 / **Revised:** 9 October 2023 / **Accepted:** 9 October 2023

ABSTRACT

Under the irradiation of ultraintense laser pulses, targets made of gas, solid, or artificial materials can generate high-energy electrons, ions, and X-rays comparable to conventional accelerators or national light source facilities. Designing and creating high-performance targets are the core problems for laser acceleration. Nanotechnology and nanomaterials can help to build ideal targets that do not exist in nature. This paper reviews the advances in exploiting carbon nanotubes as outstanding targets for laser-driven particle acceleration in memory of Prof. Sishen Xie, the inventor of the fabrication method. We hope that the successful implementation of such targets in enhanced ion acceleration, high-efficiency electron acceleration, and brilliant X-ray generation could attract more interdiscipline interests and promote the development of this field.

KEYWORDS

laser acceleration, laser-driven ion acceleration, X-ray sources, carbon nanotubes

High-energy electrons and ions are the cornerstones of nuclear science and technology. Relevant clinic and industry applications have a billions-of-dollar market that fastly grows yearly. Conventionally, they are produced in radio-frequency accelerators, which build macroscale (1–10^3 m) acceleration electric fields in the vacuum for particle acceleration. The strength of such a field, however, cannot exceed the breakdown field of metals in vacuum, e.g., maximum 10^2 V/μm. Therefore, the sizes of the accelerators are inevitably large, and accelerator-based sciences and applications are renowned for their high cost.

Since 2000, a novel particle acceleration method, laser acceleration, has developed fast and achieved great success [1–4]. Unlike in conventional accelerators, electrons and ions are accelerated in a laser-irradiated target rather than in a vacuum. Under the irradiation at an intensity over 10^{18} W/cm^2, a huge amount (10^{19}–10^{21}/cm^3) of electrons in the target are ionized and displaced. Tremendous charge separation results in an ultrastrong electric field (10^3–10^6 V/μm), orders of magnitude higher than the breakdown field in vacuum [5]. Electrons or ions injected in this field can be accelerated to high energy in μm–mm distance. Because of its potential in compact particle accelerators, laser acceleration attracts extensive interest and strongly motivates the construction of large laser facilities worldwide. Nowadays, the highest energy of laser-accelerated electrons has reached 8 GeV [6, 7], higher than that in modern synchrotron sources; near-100-MeV protons have been obtained [8, 9], which can be used for tumor therapy [10].

In laser acceleration, targets play the core role in converting laser energy to particles. The most widely used targets are gas targets and solid targets. They are ionized as plasmas by the rising edge or the pedestal of ultraintense laser pulses. Their material properties such as electrical conductivity, optical absorptance, thermal conductivity, etc., only influence the ionization process. Once turned into plasmas, the free electron density of the targets n_e predominantly determines the interaction. In a gas target, n_e is much lower than the so-called critical density of $n_c = 1.1 \times 10^{21} \lambda_L^2$ μm^2/cm^3 (λ_L is the laser wavelength), typically $n_e \sim 10^{-2} - 10^{-4} n_c$. The laser pulse can propagate in the gas without significant energy loss and excite a plasma wave (wakefield) behind itself. Electrons trapped in the wave can be stably accelerated to GeV level over a few mm through laser wakefield acceleration (LWFA) [11, 12]. However, due to the weak coupling, the laser-to-electron energy conversion efficiency in gas targets is merely 10^{-3}–10^{-5} [13, 14], which seriously limits the applications. On the contrary, solid targets, whose electron densities are hundreds of the critical density, strongly reflect the laser pulse. Thus, the interaction occurs only in the skin depth on the surface. As a result, electrons and ions cannot undergo a long-distance acceleration to high energy, typically merely at the MeV level [15].

Theory predicts that targets of the highest acceleration efficiency should have an electron density around the critical density [16], e.g. $n_e \sim n_c$. In such a "near-critical-density (NCD) " target, the plasma oscillations resonate with the laser field [17], permitting a strong absorption of the laser energy and an energy conversion efficiency to fast electrons over 50%. With the assistance of the self-generated magnetic field, the electrons can be confined near the laser axis, ensuring a long-distance direct laser acceleration (DLA). As a result, the maximum energies of the electrons are 3–10 times higher than that in solid targets [18], over

Address correspondence to wenjun.ma@pku.edu.cn

100 MeV using existing lasers and could reach GeV level under higher intensity.

Given all the atoms are fully ionized, the mass density of an NCD target would be a few mg/cm^3, just in the middle of solid and gas. For many years, considerable efforts have been made to pursue the NCD targets as they do not exist in nature. Porous materials such as foams have the right mass densities. Therefore, the attempts employing foams as NCD targets were made right after the theoretical prediction. Willingale et al. irradiate 250-μm-thick foam targets synthesized by *in situ* polymerization technique using the Vulcan Petawatt laser [19]. The composition of the foams is 71% C, 27% O, and 2% H by mass, and the mass density ranges from 3 to 100 μg/cm^3. They observed the highest protons energy of 45 MeV from the targets with the lowest density. Their numerical simulations predicted that > 100 MeV protons can be generated if the targets were perfectly homogenized. Porous carbon foams made by pulsed laser deposition were also proposed and utilized in the experiments by Prencipe et al. [20, 21]. The foams were deposited on 0.75-μm-thick Al foils, composing double-layer targets for shooting. In the optimized targets, the foam's density was about 7 μg/cm^3 and its inhomogeneity scale was improved from typical value of 5–7 μm to 0.5 μm. Comparing DLTs with simple Al foils, they observed a systematic enhancement of the maximum and average energies and number of accelerated ions. Maximum energies up to 30 MeV for protons and 130 MeV for C^{6+} ions were detected. Their three-dimensional (3D) numerical simulations revealed that, unlike in a uniform NCD plasma, the propagation of the pulse is strongly determined by the non-uniformities of the density at the micrometric scale and highly complicated. Recently, Rosmej et al. demonstrated that if CHO aerogel foam targets were pre-ionized and homogenized by a nanosecond pulse, the effective temperature of super-ponderomotive electron was enhanced to 13 MeV as a comparison to 1.5–2 MeV in the case of metallic foil [22]. The charge of electrons with energy above 30 MeV reached 78 nC. Such a high charge is highly benificial for the generation of secondary X-ray/γ-ray, and studies in high energy density physics [23] and nuclear physics [24].

The foam targets used in above and other studies were composed of micrometer-scale solid constructures [25]. As the thickness of the solid constructures far exceeds the laser skin depth, the foam cannot be fully ionized and homogenized at the wavelength scale by the laser rising edge, which would cause the deviation from expected interaction and are typically detrimental [26, 27].

Besides foam targets, gas jet with a high pressure of hundreds of bars can reach the NCD regime and intrincically homoneneous. But the laser pulses will be severely dissipated in the 100s-μm-long edge of the expanded gas jet before they arrive at the high-density region, which prevents the happending of the expected laser acceleration. Up to now, successful application of high-pressure gas jet as NCD targets for laser acceleration has not been demonstrated yet.

Since 2012, we developed a kind of nano-structured foam made of carbon nanotubes (CNT) as NCD targets for laser acceleration and demonstrated their outstanding performance. In such a target, single-walled CNT bundles (diameter of 5–10 nm, length of 5–50 μm) form a 3D nest-like architecture (Fig. 1(a)), very similar to a foam. Since 99.9% of space in the CNT foam is vacant, its bulk density is thus in the range of a few mg/cm^{-3}, perfectly matching the critical density. Figure 1(b) shows an image of a target holder covered by a layer of free-standing CNT foam. During the experiment, the laser pulses shoot through the holes of the holder and destroy the foam at the holes. A target holder like

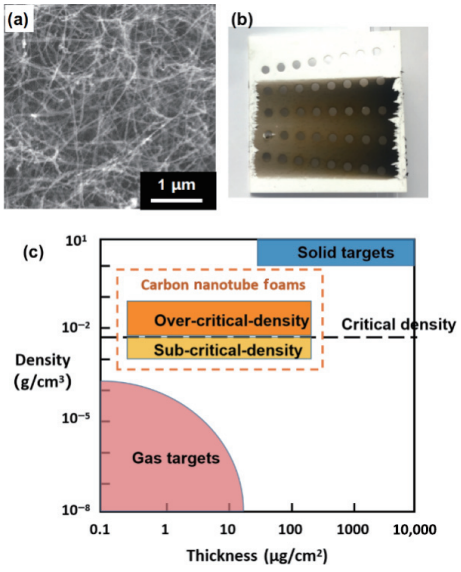

Figure 1 (a) SEM image of a carbon nanotube target. (b) A CNT foam coated on a target holder. (c) Comparison of the CNT targets with other widely-used targets in laser acceleration.

the one in Fig. 1(b) can support the continuous shooting of 40 targets in a row. By changing the growth parameter of the CNTs, the average electron density of the foam can currently be tuned between $0.2n_c$ and $2n_c$. Figure 1(c) compares the CNT targets with other widely-used targets in laser acceleration. One can see that they nicely fit the gap between the gas and solid targets.

The diameter of a CNT bundle in the CNT foams (CNF) is only 5–10 nm, smaller than the optical skin depth. So the electromagnetic screening effect is minimized, permitting the free propagation of the laser pulse in foam. We have made numerical simulations studying the evolution of targets under the irradiation of the targets [28]. According to the simulation results, an ultraintense laser pulse's picosecond scale rising edge can promptly ionize the carbon atoms and expand the CNT bundles as plasmas. Within a few hundred femtoseconds, the CNT nest no longer exists and evolves into a pursued homogenous plasma as presented in Fig. 2. Owing to the limited expansion time (< 1 ps), the density scale length at the plasma boundary is tens of nm, two orders of magnitude smaller than that of high-pressure gas jets. Such a sharp vacuum-plasma boundary efficiently avoids plasma instabilities in the density ramp and ensures an ideal interaction of the main pulse with the NCD plasma.

The fabrication method of CNT foams originated from Prof. Sishen Xie's group. In 2007, we first reported that long and branched CNT bundles can form tightly bonded laminar two-dimensional (2D) networks [29]. Figure 3 shows the growth mechanism. Firstly, the catalyst is evaporated upstream of the furnace and transferred into the high-temperature zone by Ar+CH_4 gas flow. At the high-temperature zone (1100 °C, step 2 in Fig. 3), the catalysts agglomerate as nanoparticles, which serve as the seeds of carbon nanotubes. Fed by the carbon atoms from CH_4, nanotubes grow out of the seeds and form a network near the high-temperature zone. The packed 2D networks naturally comprise a macroscale thin film with a high tensile strength of 400 Mpa [29]. Fibers made by twisting such a network have higher strength up to 800 MPa and a module of 15 GPa [30]. Such a tightly-bonded network is a perfect structure for load transfer when composited with polymers, showing order of magnitude improvement in strength compared to randomly dispersed short CNT reinforced composites because of molecular level couplings between nanotubes and polymer chains [31]. These works are

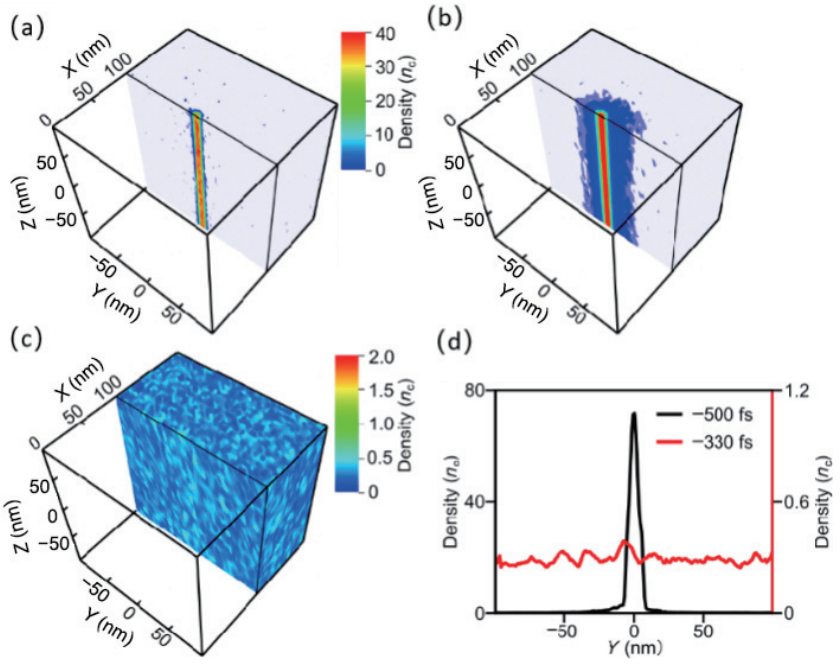

Figure 2 Simulated ionization and expansion process of one CNT bundle at (a) −670, (b) −500, and (c) −330 fs before the laser peak, respectively. A uniform NCD plasma is already formed at −330 fs. (d) Averaged electron density along the *Y*-axis at −500 and −330 fs. Reproduced with permission from Ref. [28], © Shou Y. R. et al. 2022.

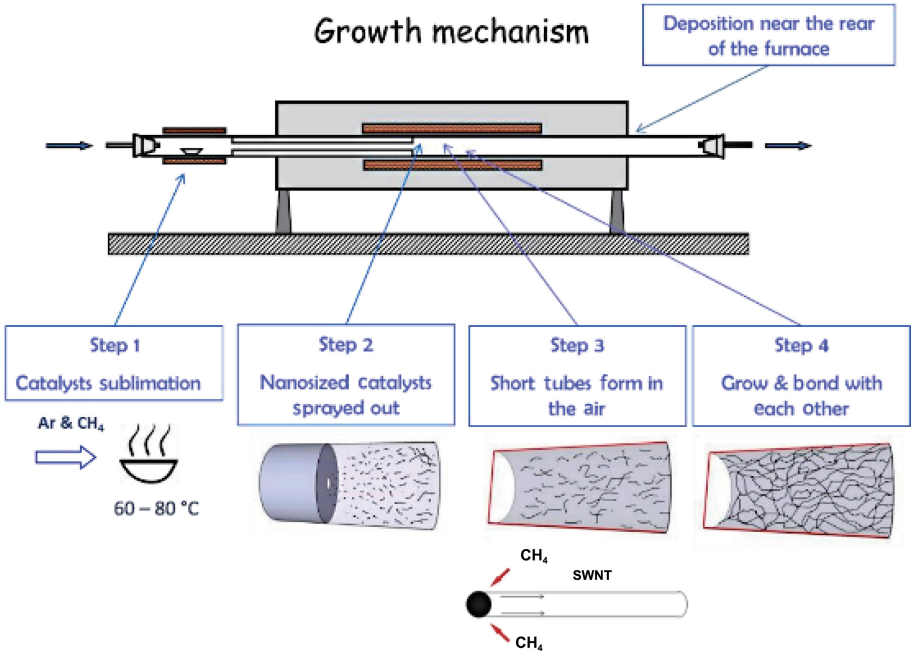

Figure 3 Growth mechanism of carbon nanotube network through FCCVD. Reproduced with permission from Ref. [38], © Szerypo, J. et al. 2019.

among the pioneers of macroscopic carbon nanotube assemblies [32, 33], expediting a series of applications later including saturable absorbers [34], electromechanical actuators [35], strain sensors [36], and supercapacitors [37].

When I worked at Ludwig-Maximilians-Universität München (LMU) as a postdoc, I found that if the CNT bundles are shorter by controlling the growth parameters, they will not form the 2D laminar network in the high-temperature zone but a 3D nest-like network in the low-temperature zone instead [38]. The macroscopic assemblies of the networks are very light and mechanically robust. One can manually transfer them to any substrate even when their thicknesses are down to tens of micrometers. With the further developed fabrication method by enlarging the diameter of the quartz tube and introducing a three-segment water cooling pipe [39], large-area (> 25 cm^2) and highly uniform CNFs were deposited on nanometer-thin metal or plastic foils as double-layer targets. The density and thickness of the CNF can be controlled in the range of 1–13 mg/cm^3 and 10–200 μm, respectively. The improved synthesis method enables the fabrication of double-layer targets composed of CNFs and ultrathin plastic and metal foils, which are highly demanded targets for laser ion acceleration and laser-driven radiation sources.

The first experimental result using CNT foam targets in laser acceleration was reported in 2015 [40]. CNT foams with a mass density of 12 mg/cm^3, e.g., the electron density of $2n_c$, were employed as plasma lenses to self-focus and steepen relativistic femtosecond pulses at the intensity of 10^{20} W/cm^2. It was found that the rising edge of the transmitted pulses after a free-standing 10-μm-thick CNF was significantly steepened to only 4 fs (Fig. 4).

The laser intensity was also increased by 10 times compared to that in the vacuum. This extremely steep-rising edge and the enhanced peak intensity provide ideal conditions for radiation pressure acceleration. By applying the shaped pulse in ion acceleration, we found that CNFs with optimal thicknesses can increase the maximum energy of carbon ions from 80 to 240 MeV. Because of the first use of CNTs in laser acceleration, this work was selected as the editor's suggestion of Physical Review Letters.

In 2019, by further reducing the density of CNF down to 2 mg/cm^3 (n_e ~ 0.3 n_c), we realize a cascaded acceleration (CA) scheme for ions (see Fig. 5(a)) [41]. It happens when a laser pulse is focused on a double-layer target composed of a tens-of-μm-thick underdense ($n_e < n_c$) CNT foam in front of an ultrathin foil. In the foam, the laser pulse produces a dense, high-energy electron flow behind itself. Once the laser pulse, followed by the electron flow, arrives at the ultrathin solid foil, ions residing in the foil undergo radiation pressure acceleration (RPA) at first, then cascaded accelerated in a long-lifetime sheath field caused by the electron flow. The superiority of CA is that the initial RPA stage gives rise to an efficient ionization and ejection of highly ionized ions, and the second acceleration stage ensures a sufficient long acceleration time. Our experimental results show that carbon ions with energy up to 580 MeV and protons up to 60 MeV can be generated using the CA scheme, about 2 times of the previous record using femtosecond lasers. According to the scaling law we obtained, 2.4 GeV carbon ions can be obtained with a 100-J femtosecond laser pulse, which is superior to other reported acceleration schemes (Fig. 5(b)).

The cascaded acceleration is highly favorable for heavy and very-heavy ion acceleration [42]. Using a petawatt (PW) laser and CNT double-layer targets, we produced deeply ionized Au with an unprecedented energy of 1.2 GeV (6.2 MeV/u) [43]. The measured charge state distribution up to 61+ revealed that laser intensity is crucial for very-heavy ion acceleration. The double-layer targets prolong the acceleration time without sacrificing the strength of the acceleration field. This work paves the way to the generation of >10 MeV/u very-heavy ions with high-repetition-rate femtosecond laser pulses, which is highly appealing for applications such as injectors for heavy ion accelerators, heavy ion fission-fusion, and the generation of warm dense matter.

Besides energetic ions, brilliant X- and γ-ray sources with ultrashort duration are widely pursued in fundamental science, industry, and medicine. Modern light source facilities can produce X-ray pulses 10^{10} times brighter than X-ray tubes by wiggling relativistic electrons from conventional accelerators. Laser acceleration can do the same in a much more compact way. Femtosecond X-ray and γ-ray sources with keV to 10 s MeV photon energies have been demonstrated by utilizing laser-accelerated electrons from gas targets in LWFA regime [44–47]. However, the laser-to-X-ray energy conversion efficiency is only 10^{-7}–10^{-5} [14], severely undermining their compatibility against other sources. CNT foams can highly efficiently produce 100-MeV-

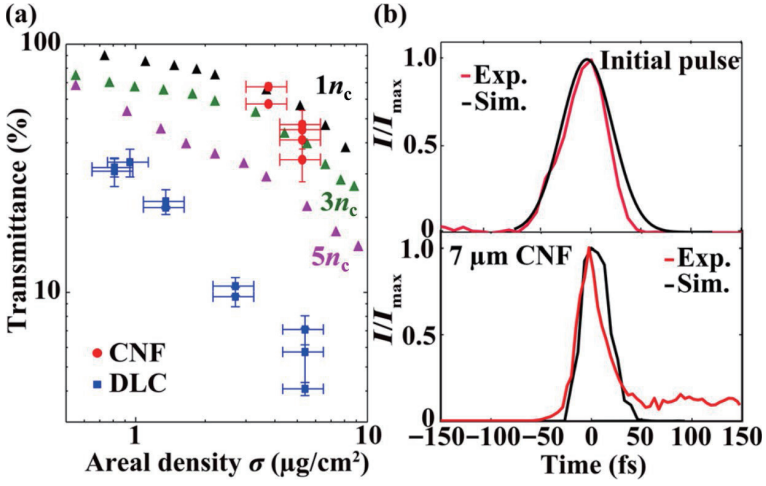

Figure 4 (a) Laser transmittance measured through CNF (red circles). The triangles with different colors represent the transmission extracted from 3D PIC simulations performed for electron densities of n_e/n_c = 1, 3, and 5. (b) Measured and simulated temporal intensity distribution evidencing pulse front steepening through a 7-μm-thick CNF target (corresponding to an areal density of σ = 5.2 μg/cm^2). Reproduced with permission from Ref. [40], © American Physical Society 2015.

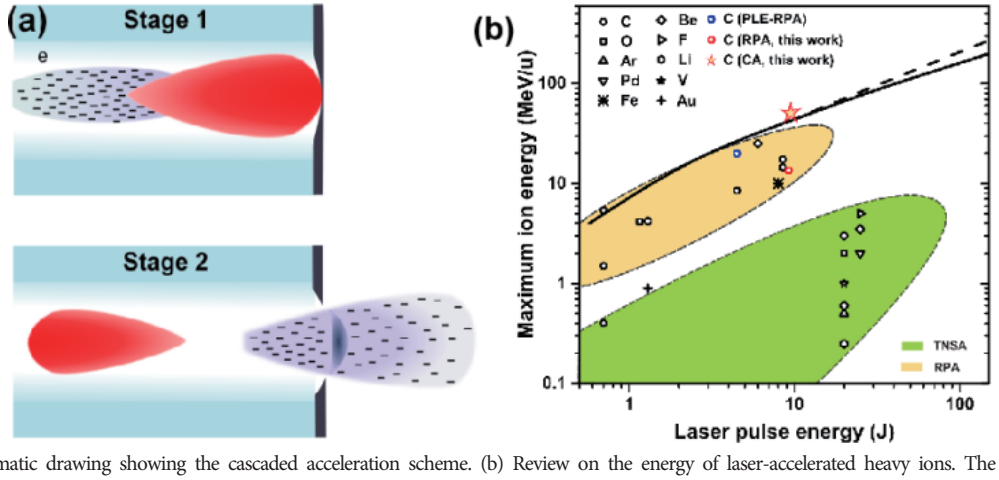

Figure 5 (a) Schematic drawing showing the cascaded acceleration scheme. (b) Review on the energy of laser-accelerated heavy ions. The results of cascaded acceleration using targets are labeled by the red circle and pentagram. Reproduced with permission from Ref. [41], © American Physical Society 2019.

level DLA electrons [48] when PW laser pulses irradiate them, which could lead to the generation of brilliant X-rays.

By exploiting CNT targets, we generated 10^{12}/shot hard X-ray photons recently, which is two orders of magnitude more than that from reported gas targets [28]. In the experiment, we utilized state-of-the-art petawatt femtosecond laser pulses with a peak intensity of 10^{21} W/cm^2 and a temporal contrast exceeding 10^{12} up to 2 ps before the main pulse. Two regimes are explored with distinctive targets as depicted in Fig. 6. In single-layer free-standing CNT targets, X-rays we generated from the synchrotron emission (SE) of the DLA electrons when they are strongly wiggled by the self-generated magnetic field (~ 10^4 T). In double-layer targets, more X-rays were generated from nonlinear Compton scattering (CS) between the DLA electrons and the laser pulse reflected from the foil [49]. The energy spectra of generated photons were measured by a combination of diagnostics at multiple angles. The measured spectra in the forward directions show a broadband feature in both regimes. The spectral intensity exceeds 10^8 photons/sr/(0.1% BW) (BW, bandwidth) at 15 keV and 10^7 photons/sr/(0.1% BW) at 100 keV in the SE regime. As a comparison, a substantial enhancement of the photon yield was observed in the CS regime, especially for the high-energy photons. The spectral intensity increases to around 10^8 photons/sr/(0.1% BW) at 100 keV, and exceeds 10^7 photons/sr/(0.1% BW) at 1 MeV.

Because the DLA electrons carry substantial transverse momentums, the emitted X-rays from CNT targets have a very large divergence angle, which is favorable for large-field-of-view X-ray imaging. The total yield of hard X-ray photons (> 30 keV) in the CS regime reaches 5.4×10^{10} photons/J, exceeding that in the LWFA region by 2–5 orders of magnitude, corresponding to an unprecedented efficiency of 10^{-3}. Moreover, our numerical simulations indicate CNT targets can deliver 10-MeV γ-rays with energy conversion efficiency exceeding 1.5% if they are irradiated by an upcoming 10-PW-class laser. Their brilliance will outperform all existing artificial γ-ray sources by two orders of magnitude [50]. Figure 7 shows the peak brilliance of X-rays as a function of photon energy and compares the results with other X-ray sources, where SE and CS represent results from single-layer and double-layer targets, respectively. One can see that their peak brilliance is comparable to or higher than that of the conventional synchrotron sources in the hard-X-ray and γ-ray range.

In summary, targets made of carbon nanotubes have shown their outstanding performance in laser-driven particle acceleration and X-ray generation because of their unique structure. Other possible applications, such as efficient ultraviolet and soft X-ray sources, are also under exploration [51]. It is reasonable to speculate that foams made of other materials instead of CNT with similar structures may also work. The biggest challenge to build a CNT-based laser-driven accelerator or an X-ray source is their low repetition rate. Current experiments are demonstrated at a single-shot level. A hertz-level repetition rate can be realized by using target wheels or tapes, but they cannot continuously run for a long time. More efforts and innovations on target fabrication and delivery methods are needed, which gives a big room for nano research.

Acknowledgements

This work was supported by the following projects: the National Natural Science Foundation of China Innovation Group Project (No. 11921006), National Grand Instrument Project (No. 2019YFF01014402), and National Science Fund for Distinguished Young Scholars (No. 12225501).

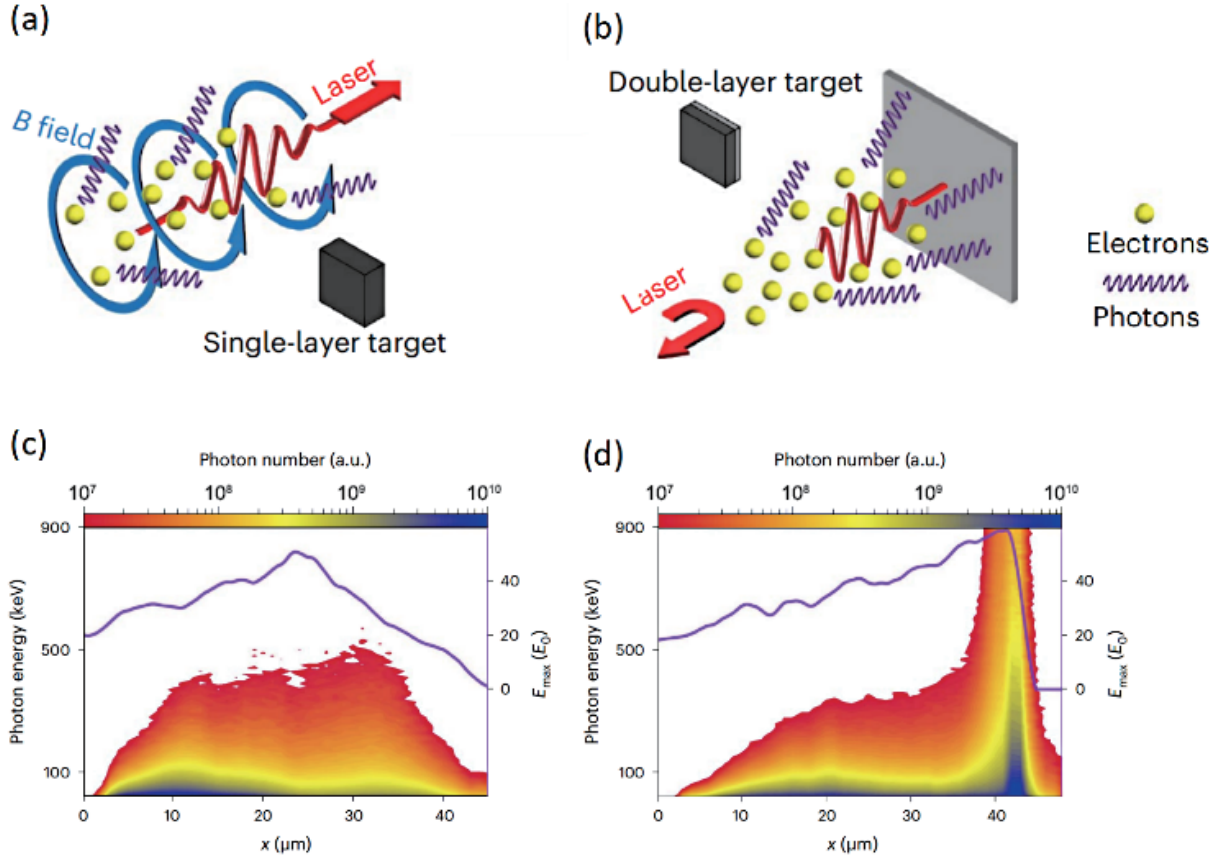

Figure 6 (a) and (b) Schematic drawings showing the X-ray generation process through synchrotron emission in a single-layer target and nonlinear Compton scattering in a double-layer target. (c) and (d) Simulations indicating the birthplaces of X-rays with different energies in the plasma channel in a single-laye target and a double-layer target, respectively. Reproduced with permission from Ref. [28], © Shou Y. R. et al. 2022.

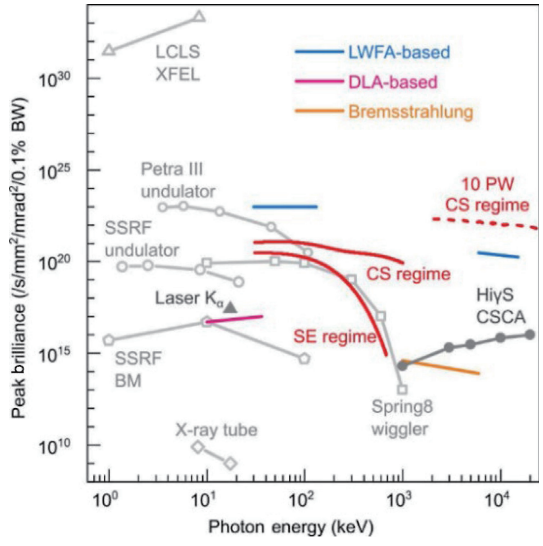

Figure 7 Comparison of the peak brilliance modified from Fig.5(a). Reproduced with permission from Ref. [28], © Shou Y. R. et al. 2022. BM: synchrotron source based on bending magnets. Wiggler and undulator: third-generation X-ray source using wigglers or undulators. XFEL: X-ray free-electron laser. CSCA: γ-ray source based on Compton scattering of electrons from conventional accelerators. LWFA: laser-wakefield accelerated electrons from gas targets.

References

[1] Snavely, R. A.; Key, M. H.; Hatchett, S. P.; Cowan, T. E.; Roth, M.; Phillips, T. W.; Stoyer, M. A.; Henry, E. A.; Sangster, T. C.; Singh, M. S. et al. Intense high-energy proton beams from Petawatt-laser irradiation of solids. *Phys. Rev. Lett.* **2000**, *85*, 2945–2948.

[2] Mangles, S. P. D.; Murphy, C. D.; Najmudin, Z.; Thomas, A. G. R.; Collier, J. L.; Dangor, A. E.; Divall, E. J.; Foster, P. S.; Gallacher, J. G.; Hooker, C. J. et al. Monoenergetic beams of relativistic electrons from intense laser–plasma interactions. *Nature* **2004**, *431*, 535–538.

[3] Geddes, C. G. R.; Toth, C.; van Tilborg, J.; Esarey, E.; Schroeder, C. B.; Bruhwiler, D.; Nieter, C.; Cary, J.; Leemans, W. P. High-quality electron beams from a laser wakefield accelerator using plasma-channel guiding. *Nature* **2004**, *431*, 538–541.

[4] Faure, J.; Glinec, Y.; Pukhov, A.; Kiselev, S.; Gordienko, S.; Lefebvre, E.; Rousseau, J. P.; Burgy, F.; Malka, V. A laser-plasma accelerator producing monoenergetic electron beams. *Nature* **2004**, *431*, 541–544.

[5] Mourou, G. A.; Tajima, T.; Bulanov, S. V. Optics in the relativistic regime. *Rev. Mod. Phys.* **2006**, *78*, 309–371.

[6] Gonsalves, A. J.; Nakamura, K.; Daniels, J.; Benedetti, C.; Pieronek, C.; de Raadt, T. C. H.; Steinke, S.; Bin, J. H.; Bulanov, S. S.; van Tilborg, J. et al. Petawatt laser guiding and electron beam acceleration to 8 GeV in a laser-heated capillary discharge waveguide. *Phys. Rev. Lett.* **2019**, *122*, 084801.

[7] Leemans, W. P.; Gonsalves, A. J.; Mao, H. S.; Nakamura, K.; Benedetti, C.; Schroeder, C. B.; Tóth, C.; Daniels, J.; Mittelberger, D. E.; Bulanov, S. S. et al. Multi-GeV electron beams from capillary-discharge-guided subpetawatt laser pulses in the self-trapping regime. *Phys. Rev. Lett.* **2014**, *113*, 245002.

[8] Higginson, A.; Gray, R. J.; King, M.; Dance, R. J.; Williamson, S. D. R.; Butler, N. M. H.; Wilson, R.; Capdessus, R.; Armstrong, C.; Green, J. S. et al. Near-100 MeV protons via a laser-driven transparency-enhanced hybrid acceleration scheme. *Nat. Commun.* **2018**, *9*, 724.

[9] Ma, W. J.; Liu, Z. P.; Wang, P. J.; Zhao, J. R.; Yan, X. Q. Experimental progress of laser-driven high-energy proton acceleration and new acceleration schemes. *Acta Phys. Sin.* **2021**, *70*, 084102.

[10] Ledingham, K. W. D.; Bolton, P. R.; Shikazono, N.; Ma, C. M. C. Towards laser driven hadron cancer radiotherapy: A review of progress. *Appl. Sci.* **2014**, *4*, 402–443.

[11] Lu, W.; Tzoufras, M.; Joshi, C.; Tsung, F. S.; Mori, W. B.; Vieira, J.; Fonseca, R. A.; Silva, L. O. Generating multi-GeV electron bunches using single stage laser wakefield acceleration in a 3D nonlinear regime. *Phys. Rev. ST Accel. Beams* **2007**, *10*, 061301.

[12] Pukhov, A.; Meyer-ter-Vehn, J. Laser wake field acceleration: The highly non-linear broken-wave regime. *Appl. Phys. B* **2002**, *74*, 355–361.

[13] Esarey, E.; Schroeder, C. B.; Leemans, W. P. Physics of laser-driven plasma-based electron accelerators. *Rev. Mod. Phys.* **2009**, *81*, 1229–1285.

[14] Corde, S.; Phuoc, K. T.; Lambert, G.; Fitour, R.; Malka, V.; Rousse, A.; Beck, A.; Lefebvre, E. Femtosecond X rays from laser-plasma accelerators. *Rev. Mod. Phys.* **2013**, *85*, 1–48.

[15] Daido, H.; Nishiuchi, M.; Pirozhkov, A. S. Review of laser-driven ion sources and their applications. *Rep. Prog. Phys.* **2012**, *75*, 056401.

[16] Pukhov, A.; Sheng, Z. M.; Meyer-ter-Vehn, J. Particle acceleration in relativistic laser channels. *Phys. Plasmas* **1999**, *6*, 2847–2854.

[17] Pukhov, A.; Meyer-ter-Vehn, J. Relativistic magnetic self-channeling of light in near-critical plasma: Three-dimensional particle-in-cell simulation. *Phys. Rev. Lett.* **1996**, *76*, 3975–3978.

[18] Robinson, A. P. L.; Arefiev, A. V.; Neely, D. Generating "superponderomotive" electrons due to a non-wake-field interaction between a laser pulse and a longitudinal electric field. *Phys. Rev. Lett.* **2013**, *111*, 065002.

[19] Willingale, L.; Nagel, S. R.; Thomas, A. G. R.; Bellei, C.; Clarke, R. J.; Dangor, A. E.; Heathcote, R.; Kaluza, M. C.; Kamperidis, C.; Kneip, S. et al. Characterization of high-intensity laser propagation in the relativistic transparent regime through measurements of energetic proton beams. *Phys. Rev. Lett.* **2009**, *102*, 125002.

[20] Prencipe, I.; Sgattoni, A.; Dellasega, D.; Fedeli, L.; Cialfi, L.; Choi, I. W.; Kim, I. J.; Janulewicz, K. A.; Kakolee, K. F.; Lee, H. W. et al. Development of foam-based layered targets for laser-driven ion beam production. *Plasma Phys. Control. Fusion* **2016**, *58*, 034019.

[21] Prencipe, I.; Metzkes-Ng, J.; Pazzaglia, A.; Bernert, C.; Dellasega, D.; Fedeli, L.; Formenti, A.; Garten, M.; Kluge, T.; Kraft, S. et al. Efficient laser-driven proton and bremsstrahlung generation from cluster-assembled foam targets. *New J. Phys.* **2021**, *23*, 093015.

[22] Rosmej, O. N.; Andreev, N. E.; Zaehter, S.; Zahn, N.; Christ, P.; Borm, B.; Radon, T.; Sokolov, A.; Pugachev, L. P.; Khaghani, D. et al. Interaction of relativistically intense laser pulses with long-scale near critical plasmas for optimization of laser based sources of MeV electrons and gamma-rays. *New J. Phys.* **2019**, *21*, 043044.

[23] Rosmej, O. N.; Gyrdymov, M.; Günther, M. M.; Andreev, N. E.; Tavana, P.; Neumayer, P.; Zähter, S.; Zahn, N.; Popov, V. S.; Borisenko, N. G. et al. High-current laser-driven beams of relativistic electrons for high energy density research. *Plasma Phys. Control. Fusion* **2020**, *62*, 115024.

[24] Lan, H. Y.; Wu, D.; Liu, J. X.; Zhang, J. Y.; Lu, H. G.; Lv, J. F.; Wu, X. Z.; Luo, W.; Yan, X. Q. Photonuclear production of nuclear isomers using bremsstrahlung induced by laser-wakefield electrons. *Nucl. Sci. Tech.* **2023**, *34*, 74.

[25] Prencipe, I.; Fuchs, J.; Pascarelli, S.; Schumacher, D. W.; Stephens, R. B.; Alexander, N. B.; Briggs, R.; Büscher, M.; Cernaianu, M. O.; Choukourov, A. et al. Targets for high repetition rate laser facilities: Needs, challenges and perspectives. *High Power Laser Sci. Eng.* **2017**, *5*, e17.

[26] Tikhonchuk, V.; Gu, Y. J.; Klimo, O.; Limpouch, J.; Weber, S. Studies of laser-plasma interaction physics with low-density targets for direct-drive inertial confinement schemes. *Matter Radiat. Extremes* **2019**, *4*, 045402.

[27] Fedeli, L.; Formenti, A.; Cialfi, L.; Pazzaglia, A.; Passoni, M. Ultra-intense laser interaction with nanostructured near-critical plasmas. *Sci. Rep.* **2018**, *8*, 3834.

[28] Shou, Y. R.; Wang, P. J.; Lee, S. G.; Rhee, Y. J.; Lee, H. W.; Yoon, J. W.; Sung, J. H.; Lee, S. K.; Pan, Z.; Kong, D. F. et al. Brilliant femtosecond-laser-driven hard X-ray flashes from carbon nanotube plasma. *Nat. Photonics* **2023**, *17*, 137–142.

[29] Ma, W. J.; Song, L.; Yang, R.; Zhang, T. H.; Zhao, Y. C.; Sun, L. F.; Ren, Y.; Liu, D. F.; Liu, L. F.; Shen, J. et al. Directly synthesized strong, highly conducting, transparent single-walled carbon nanotube films. *Nano Lett.* **2007**, *7*, 2307–2311.

[30] Ma, W. J.; Liu, L. Q.; Yang, R.; Zhang, T. H.; Zhang, Z.; Song, L.; Ren, Y.; Shen, J.; Niu, Z. Q.; Zhou, W. Y. et al. Monitoring a micromechanical process in macroscale carbon nanotube films and fibers. *Adv. Mater.* **2009**, *21*, 603–608.

[31] Ma, W. J.; Liu, L. Q.; Zhang, Z.; Yang, R.; Liu, G.; Zhang, T. H.; An, X. F.; Yi, X. S.; Ren, Y.; Niu, Z. Q. et al. High-strength composite fibers: Realizing true potential of carbon nanotubes in polymer matrix through continuous reticulate architecture and molecular level couplings. *Nano Lett.* **2009**, *9*, 2855–2861.

[32] Liu, L. Q.; Ma, W. J.; Zhang, Z. Macroscopic carbon nanotube assemblies: Preparation, properties, and potential applications. *Small* **2011**, *7*, 1504–1520.

[33] Zhou, W. Y.; Bai, X. D.; Wang, E. G.; Xie, S. S. Synthesis, structure, and properties of single-walled carbon nanotubes. *Adv. Mater.* **2009**, *21*, 4565–4583.

[34] Ma, W. J.; Feng, B. H.; Ren, Y.; Zeng, Q. S.; Niu, Z. Q.; Li, J. Z.; Zhang, X. X.; Dong, H. B.; Zhou, W. Y.; Xie, S. S. Large third-order optical nonlinearity in directly synthesized single-walled carbon nanotube films. *J. Nanosci. Nanotechnol.* **2010**, *10*, 7333–7335.

[35] Li, J. Z.; Ma, W. J.; Song, L.; Niu, Z. Q.; Cai, L.; Zeng, Q. S.; Zhang, X. X.; Dong, H. B.; Zhao, D.; Zhou, W. Y. et al. Superfast-response and ultrahigh-power-density electromechanical actuators based on hierarchal carbon nanotube electrodes and chitosan. *Nano Lett.* **2011**, *11*, 4636–4641.

[36] Gao, Y.; Li, J. Z.; Liu, L. Q.; Ma, W. J.; Zhou, W. Y.; Xie, S. S.; Zhang, Z. Axial compression of hierarchically structured carbon nanotube fiber embedded in epoxy. *Adv. Funct. Mater.* **2010**, *20*, 3797–3803.

[37] Niu, Z. Q.; Zhou, W. Y.; Chen, J.; Feng, G. X.; Li, H.; Ma, W. J.; Li, J. Z.; Dong, H. B.; Ren, Y.; Zhao, D. et al. Compact-designed supercapacitors using free-standing single-walled carbon nanotube films. *Energy Environ. Sci.* **2011**, *4*, 1440–1446.

[38] Szerypo, J.; Ma, W.; Bothmann, G.; Hahner, D.; Haug, M.; Hilz, P.; Kreuzer, C.; Lange, R.; Seuferling, S.; Speicher, M. et al. Target fabrication for laser-ion acceleration research at the Technological Laboratory of the LMU Munich. *Matter Radiat. Extremes* **2019**, *4*, 035201.

[39] Wang, P. J.; Qi, G. J.; Pan, Z.; Kong, D. F.; Shou, Y. R.; Liu, J. B.; Cao, Z. X.; Mei, Z. S.; Xu, S. R.; Liu, Z. P. et al. Fabrication of large-area uniform carbon nanotube foams as near-critical-density targets for laser-plasma experiments. *High Power Laser Sci. Eng.* **2021**, *9*, e29.

[40] Bin, J. H.; Ma, W. J.; Wang, H. Y.; Streeter, M. J. V.; Kreuzer, C.; Kiefer, D.; Yeung, M.; Cousens, S.; Foster, P. S.; Dromey, B. et al. Ion acceleration using relativistic pulse shaping in near-critical-density plasmas. *Phys. Rev. Lett.* **2015**, *115*, 064801.

[41] Ma, W. J.; Kim, I. J.; Yu, J. Q.; Choi, I. W.; Singh, P. K.; Lee, H. W.; Sung, J. H.; Lee, S. K.; Lin, C.; Liao, Q. et al. Laser acceleration of highly energetic carbon ions using a double-layer target composed of slightly underdense plasma and ultrathin foil. *Phys. Rev. Lett.* **2019**, *122*, 014803.

[42] Mei, Z. S.; Pan, Z.; Liu, Z. P.; Xu, S. R.; Shou, Y. R.; Wang, P. J.; Cao, Z. X.; Kong, D. F.; Liang, Y. L.; Peng, Z. Y. et al. Energetic laser-driven proton beams from near-critical-density double-layer targets under moderate relativistic intensities. *Phys. Plasmas* **2023**, *30*, 033107.

[43] Wang, P. J.; Gong, Z.; Lee, S. G.; Shou, Y. R.; Geng, Y. X.; Jeon, C.; Kim, I. J.; Lee, H. W.; Yoon, J. W.; Sung, J. H. et al. Super-heavy ions acceleration driven by ultrashort laser pulses at ultrahigh intensity. *Phys. Rev. X* **2021**, *11*, 021049.

[44] Kneip, S.; Nagel, S. R.; Bellei, C.; Bourgeois, N.; Dangor, A. E.; Gopal, A.; Heathcote, R.; Mangles, S. P. D.; Marquès, J. R.; Maksimchuk, A. et al. Observation of synchrotron radiation from electrons accelerated in a petawatt-laser-generated plasma cavity. *Phys. Rev. Lett.* **2008**, *100*, 105006.

[45] Cipiccia, S.; Islam, M. R.; Ersfeld, B.; Shanks, R. P.; Brunetti, E.; Vieux, G.; Yang, X.; Issac, R. C.; Wiggins, S. M.; Welsh, G. H. et al. Gamma-rays from harmonically resonant betatron oscillations in a plasma wake. *Nat. Phys.* **2011**, *7*, 867–871.

[46] Cole, J. M.; Wood, J. C.; Lopes, N. C.; Poder, K.; Abel, R. L.; Alatabi, S.; Bryant, J. S. J.; Jin, A.; Kneip, S.; Mecseki, K. et al. Laser-wakefield accelerators as hard X-ray sources for 3D medical imaging of human bone. *Sci. Rep.* **2015**, *5*, 13244.

[47] Khrennikov, K.; Wenz, J.; Buck, A.; Xu, J.; Heigoldt, M.; Veisz, L.; Karsch, S. Tunable all-optical quasimonochromatic Thomson X-ray source in the nonlinear regime. *Phys. Rev. Lett.* **2015**, *114*, 195003.

[48] Bin, J. H.; Yeung, M.; Gong, Z.; Wang, H. Y.; Kreuzer, C.; Zhou, M. L.; Streeter, M. J. V.; Foster, P. S.; Cousens, S.; Dromey, B. et al. Enhanced laser-driven ion acceleration by superponderomotive electrons generated from near-critical-density Plasma. *Phys. Rev. Lett.* **2018**, *120*, 074801.

[49] Liu, J. B.; Yu, J. Q.; Shou, Y. R.; Wang, D. H.; Hu, R. H.; Tang, Y. H.; Wang, P. J.; Cao, Z. X.; Mei, Z. S.; Lin, C. et al. Generation of bright γ-ray/hard X-ray flash with intense femtosecond pulses and double-layer targets. *Phys. Plasmas* **2019**, *26*, 033109.

[50] Macchi, A.; Pegoraro, F. Lighting up a nest for X-ray emission. *Nat. Photonics* **2023**, *17*, 129–130.

[51] Shou, Y. R.; Wang, D. H.; Wang, P. J.; Liu, J. B.; Cao, Z. X.; Mei, Z. S.; Xu, S. R.; Pan, Z.; Kong, D. F.; Qi, G. J. et al. High-efficiency generation of narrowband soft X rays from carbon nanotube foams irradiated by relativistic femtosecond lasers. *Opt. Lett.* **2021**, *46*, 3969–3972.